



Simulated Brain Tumor Growth Dynamics Using a Three-Dimensional Cellular Automaton

A. R. KANSAL*, S. TORQUATO*†‡, G. R. HARSH IV§,
E. A. CHIOCCA||** AND T. S. DEISBOECK||**††

*Department of Chemical Engineering, Department of Chemistry, †Princeton Materials Institute, Princeton University, Princeton, NJ 08544, U.S.A., §Department of Neurosurgery, Stanford University Medical School, Stanford, CA 94305, U.S.A., ||Neurosurgical Service, ¶Brain Tumor Center, **Molecular Neuro-Oncology Laboratory, Massachusetts General Hospital East, Harvard Medical School, Charlestown, MA 02129, U.S.A.

(Received on 20 August 1999, Accepted in revised form on 14 January 2000)

We have developed a novel and versatile three-dimensional cellular automaton model of brain tumor growth. We show that macroscopic tumor behavior can be realistically modeled using microscopic parameters. Using only four parameters, this model simulates Gompertzian growth for a tumor growing over nearly three orders of magnitude in radius. It also predicts the composition and dynamics of the tumor at selected time points in agreement with medical literature. We also demonstrate the flexibility of the model by showing the emergence, and eventual dominance, of a second tumor clone with a different genotype. The model incorporates several important and novel features, both in the rules governing the model and in the underlying structure of the model. Among these are a new definition of how to model proliferative and non-proliferative cells, an isotropic lattice, and an adaptive grid lattice.

© 2000 Academic Press

1. Introduction

The incidence of primary malignant brain tumors is already 8/100 000 persons per year and is still increasing. The vast majority (80%) consists of high-grade malignant neuroepithelial tumors such as glioblastoma multiforme (GBM) (Fig. 1) (Annegers *et al.*, 1981; Werner *et al.*, 1995). In spite of aggressive conventional and advanced treatments, the prognosis remains uniformly fatal with a median survival time for patients with

GBM of 8 months (Black, 1991; Whittle, 1996). The main reason for this grim outcome is not only the rapid tumor growth but especially the fact that, long before the neoplasm can be diagnosed, it has already grossly invaded the surrounding brain parenchyma, rendering surgical removal virtually ineffective. The proposed sequence of proliferation, then invasion, followed by proliferation again suggests that invasive cells left behind after an operation not only cause parenchyma destruction, but also eventually tumor recurrence (Suh & Weiss, 1984; Burger *et al.*, 1988; Nazzaro & Neuwelt, 1990; Silbergeld & Chicoine, 1997). Anti-proliferative treatments fail because of poor transport across the

‡ Author to whom correspondence should be addressed.
E-mail: torquato@matter.princeton.edu

†† T. S. Deisboeck, M.D. is also affiliated with the Department of Neurosurgery, University of Munich (Germany).

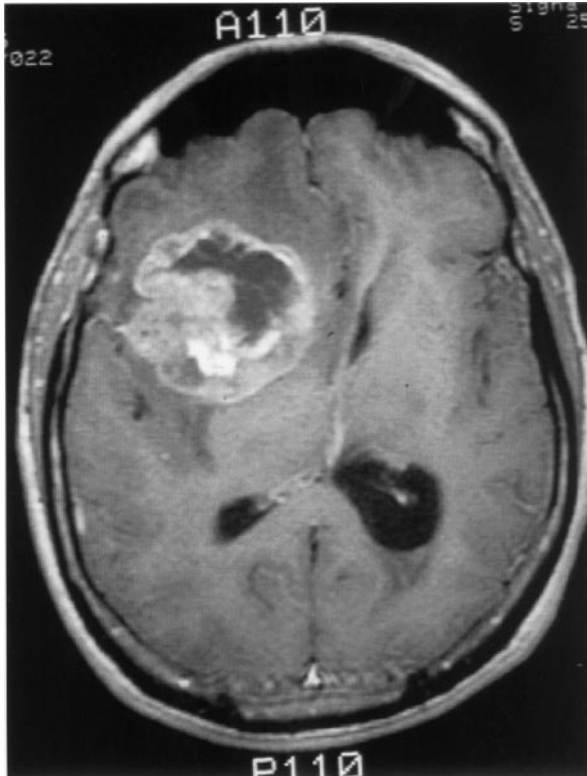


FIG. 1. T1-contrast enhanced brain MRI-scan showing a right frontal GBM tumor. Perifocal hypointensity is caused by significant edema formation. The hyper-intense, white region (ring-enhancement) reflects an area of extensive blood-brain/tumor barrier leakage. Since this regional neovascular setting provides tumor cells with sufficient nutrition it contains the highly metabolizing e.g. dividing, tumor cells (Selker *et al.*, 1982; Burger *et al.*, 1983; Kelly *et al.*, 1987; Earnest IV *et al.*, 1988). Therefore, this area corresponds to the outermost concentric shell of highly proliferating neoplastic cells in our model (see Fig. 6).

blood-brain barrier, acquired treatment resistance, and lack of susceptibility of single invading cells due to their minimal proliferative activity (Giese *et al.*, 1996; Schiffer *et al.*, 1997).

The rapid growth and resilience of tumors make it difficult to believe that they behave as random, disorganized and diffuse cell masses and suggests instead that they are *emerging, opportunistic systems*. If this hypothesis holds true, the growing tumor and not only the single cell (Kraus & Wolf, 1993) must be investigated and treated as a *self-organizing complex dynamic system*. This cannot be done with currently available *in vitro/in vivo* models or common mathematical approaches. Therefore, there is a need

for novel computational models to simulate the mechanistic complexity of solid tumor growth and invasion, combining a range of disciplines including medical, engineering and statistical physics research.

Here we report the first step towards a complex self-organizing tumor model focusing on volumetric growth of a solid tumor as the necessary precondition for subsequent and ongoing invasion. We have developed a three-dimensional cellular automaton (CA) model which describes tumor growth as a function of time. The algorithm takes into account that this growth starts out from a few cells, passes through a multicellular tumor spheroid (MTS) stage (Fig. 2) and proceeds to the macroscopic stages at clinically designated time-points for a virtual patient: detectable lesion, diagnosis and death (Sutherland, 1988; Mueller-Klieser, 1997). This simplified growth approach models macroscopic GBM tumors as an enormous idealized MTS, mathematically described by a Gompertz function (Brunton & Wheldon, 1977; Vaidya & Alexandro Jr., 1982; Norton, 1988; Marusic *et al.*, 1994). Modeling the ideal tumor at every step as an oversized spheroid is especially suited for GBM, since this tumor, like a large MTS, comprises large areas of central necrosis surrounded by a rapidly expanding shell of viable cells (Fig. 1). In accordance with experimental data, the algorithm also implicitly takes into account that invasive cells are continually shed from the tumor surface. Future work will treat the invasive dynamics explicitly.

The simulation contains several features novel to the simulation of tumor growth:

- The ability of cells to divide is treated in a new manner. By redefining the transition between dividing and non-dividing cells, it is possible to generate medically realistic overall tumor growth rates using a biologically reasonable cell-doubling time.
- Previous researchers have used the Voronoi tessellation in histopathological image analysis of tumors (Preston Jr. & Siderits, 1992; Kiss *et al.*, 1995; Haroske *et al.*, 1996). However, the present work represents the first use of the Voronoi tessellation (described later in the text) to study the dynamics of tumor

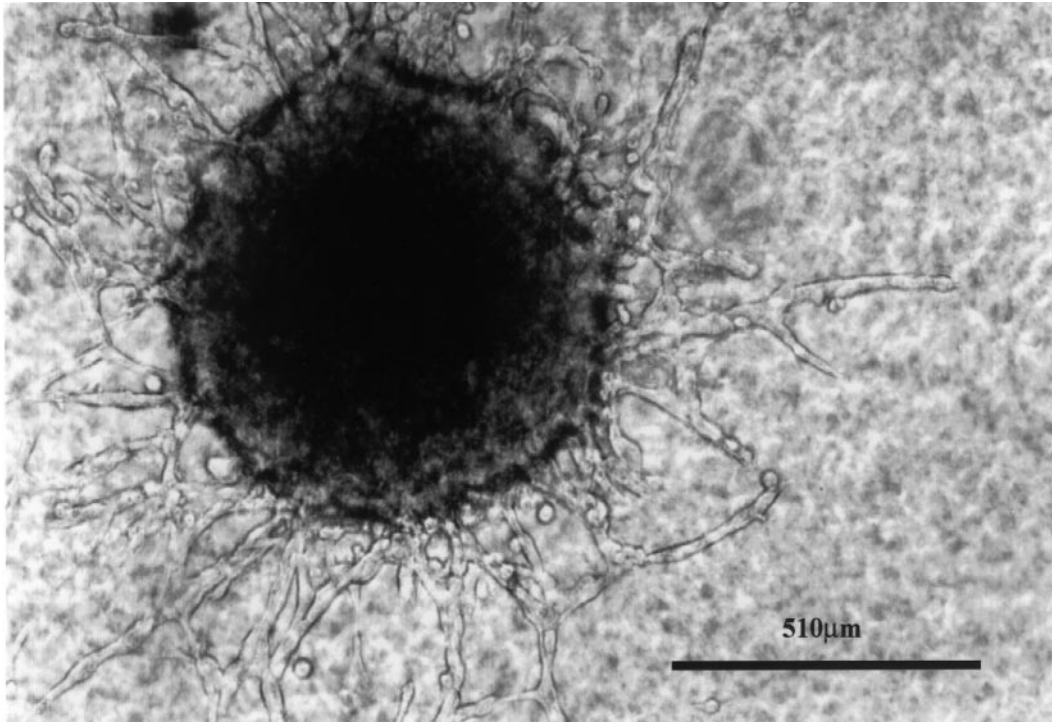


FIG. 2. MTS-gel assay showing a central spheroid with multiple “chain”-like invasion pathways leading towards the boundary (magnification: $\times 200$).

growth in a cellular automaton. This tessellation is isotropic in space and hence does not create the artificial anisotropies possible with square or cubic lattices, which have typically been used in tumor simulations.

- The model uses a varying density of lattice sites (an adaptive grid lattice). This allows small tumors to be simulated with greater accuracy, while still allowing the tumor to grow to a large size. Using this variable-density lattice, tumors can be simulated over nearly three orders of magnitude in radius.

A CA model treats the discrete nature of actual cells realistically, giving it great adaptability in treating complex situations (Kauffman, 1984; Wolfram, 1984). For example, the addition of a blood vessel or other growth promoting heterogeneity could be studied by altering a single parameter. Similarly, the effect of the surgical removal of a portion of the tumor could be readily modeled. Most importantly, a discrete model readily allows the inclusion of a number of distinct subpopulations, corresponding to different

cell clones. In addition, this work is intended to serve as a preliminary step to modeling systemic invasive growth dynamics, the nature of which is ideally suited to study using discrete modeling. Finally, each site in a CA model can be thought of as a group of actual cells. This interpretation allows the model to serve as an intuitive complement to the results obtained from a continuum model.

The simulation is designed to predict clinically important criteria such as the fraction of the tumor which is able to divide (GF), the non-proliferative (G_0/G_1 arrest) and necrotic fractions, as well as the rate of growth (volumetric doubling time) at given radii. The simulation results reflect a test case derived from the medical literature very well, proving the hypothesis that macroscopic tumor growth behavior may be modeled with primarily microscopic data. Current limitations and potential implications of this model for further tumorigenesis research are discussed. Since an approach claiming to model malignant tumor complexity must take into account cell invasion, we will also briefly describe

initial theoretical considerations to model tumor cell invasion.

In summary, our model is characterized by several biologically important features:

- The model is able to grow the tumor from a very small size of roughly 1000 real cells through to a fully developed tumor with 10^{11} cells. This allows a tumor to be grown from almost any starting point, through to maturity.
- The thickness of different tumor layers, i.e. the proliferative rim and the non-proliferative shell, are linked to the overall tumor radius by a $2/3$ power relation. This reflects a surface-area-to-volume ratio, which can be biologically interpreted as nutrients diffusing through a surface.
- Our inclusion of mechanical confinement pressure enables us to simulate the physiological confinement by the skull at different locations within the brain differently.
- The discrete nature of the model and the variable density lattice allow us to control the inclusion of mutant “hot spots” in the tumor, i.e. consider genetic instability and emergence of clonal subpopulations. The variable density lattice will allow us to look at such an area at a higher resolution.

In the following section (Section 2), we outline some of the earlier work that has been done in the field of tumor modeling. Section 3 discusses the details of the procedure for the simulation. A summary of our results is contained in Section 4. This is followed by a discussion and concluding remarks regarding our current work, as well as future work, in Section 5.

2. Previous Work

Significant research has been done in the modeling of tumors using theoretical models and computer simulations. Previous modeling has been done on a range of tumor behaviors, including proliferative growth of the tumor core (see references immediately below), invasive growth (Tracqui, 1995; Perumpanani *et al.*, 1996) and immune response (Sherratt & Nowak, 1992). Here we will focus on works which have explicitly

modeled the proliferative growth of the tumor core.

Some of the earliest work in modeling of tumors using a three-dimensional cellular automaton on a cubic lattice was carried out by Düchting & Vogelsaenger (1985) for very small tumors. These automaton rules were designed to reflect nutritional needs for tumor growth. Other important factors, such as surrounding cells and mechanical pressure, however, remained unconsidered.

Qi *et al.* (1993) considered a two-dimensional cellular automaton tumor model that reproduced idealized Gompertz results. However, cells could only divide if one of their nearest neighbors was empty. This created an unrealistically small fraction of a tumor which may divide. Furthermore, dead tumor cells were assumed to simply dissolve away rather than accumulating into a necrotic core, as is seen in real tumors. In addition, the transition from dividing cells to the resting state was handled in a purely stochastic manner, rather than the more biologically reasonable nutrient-based method used by Düchting and Vogelsaenger.

Recent work by Smolle & Stettner (1993) showed that the macroscopic behavior of a tumor can be affected by the presence of growth factors at the microscopic level and added the concept of cellular migration to the behavior of the cells. The work done by Smolle and Stettner, however, was qualitative and designed to show the range of behaviors obtainable from a simple model. Recent work has been carried out to estimate the model parameters needed to generate a given configuration (Smolle, 1998). This model, as well as those designed by Qi *et al.* and Düchting and Vogelsaenger, relied on an underlying square (or cubic) lattice. While this provides a simple method of organizing the automata, it introduces undesirable asymmetries and other artificial lattice effects.

Other researchers have attempted to study the growth patterns of tumors in a more macroscopic fashion. The work of Wasserman *et al.* (1996) used a finite element analysis technique to describe the macroscopic behavior of a tumor based on stresses imposed by various factors. Wasserman’s approach is similar to that of Chaplain & Sleeman (1993), in which the authors used

nonlinear elasticity theory to model a tumor. In that paper, the growth of the tumor was governed by a strain-energy function.

Another approach that has been taken by a number of researchers is to create equations which describe the tumor phenomenologically. The best known is the Gompertz model, which describes the volume, V , of a tumor vs. time, t , as

$$V = V_0 \exp\left(\frac{A}{B}(1 - \exp(-Bt))\right), \quad (1)$$

where V_0 is the volume at time $t = 0$ and A and B are parameters (Steel, 1977). Qualitatively, this equation gives exponential growth at small times which then saturates at large times (decelerating growth). Many tumors, however, contain more than one clonal population. A second population might have different division rates and nutritional needs, resulting in competitive effects which cannot be accounted for by the Gompertz model. The Jansson–Revesz equations model the interaction of two populations in a competitive setting (Cruywagen *et al.*, 1995). These equations are essentially the classical Lotka–Volterra equations of logistic growth with an added term to account for the conversion of one species to the other. Work by Cruywagen *et al.* has sought to apply the Jansson–Revesz equations to tumor growth. In addition, they have included a diffusive term to each equation, to account for passive cellular motion. These mathematical models are useful to describe the general size of a tumor under relatively simple conditions (two populations, Fickian diffusion), but have yet to be extended to multiple populations or active cellular motility. A review of several other mathematical models is contained in Marusic *et al.* (1994).

Finally, the growth of the tumor core has been modeled in a continuum setting using differential equations with explicit spatial dependence by several researchers. Adam (1986) used an ordinary differential equation, which reflects mass conservation of tumor cells, coupled with a reaction-diffusion equation, reflecting the distribution of nutrients within the tumor. Ward & King (1997) used nonlinear partial differential equations to generate profiles for growth of an avascular tumor based on a nutrient distribution. More

recently, Byrne & Chaplain (1998) have proposed a model which also includes the effects of nutrient diffusion and incorporates both apoptosis and necrosis explicitly. Other models, notably those by Tracqui *et al.* (1995) and Woodward *et al.* (1996), attempt to model both tumor growth and the impact of treatment.

3. Simulation Procedure

The underlying lattice for our algorithm is the Delaunay triangulation, which is the dual lattice of the Voronoi tessellation (Okabe *et al.*, 1992). The lattice generation is accomplished by first choosing a set of sites, which are simply points distributed in space according to some random process. Each cell in the final Voronoi lattice will contain one of these sites. The cell is then defined by the region of space nearer to that particular site than to any other site. In two spatial dimensions, a Voronoi lattice is a collection of such polygons, which fill the plane. This is illustrated in Fig. 3. In the three-dimensional analog, the Voronoi cells take the form of polyhedra.

The Delaunay lattice is generated from the Voronoi network by connecting those sites whose polyhedra (in three dimensions) share a common face. This determines which sites are nearest neighbors of one another. All references to nearest neighbors in this paper refer to those determined in this way. A two-dimensional analog of this is also depicted in Fig. 3.

For our algorithm, a prescribed number of random points in space are generated. The speed and memory requirements of the subsequent programs are strongly dependent on the number of points chosen. In addition, however, the larger the number of points chosen, the more accurate the model. As such, the largest number of points that can be accommodated in computer memory and run in a reasonable length of time has been used.

Because a real brain tumor grows over several orders of magnitude in volume, the lattice was designed with a variable grid size. In our lattice, the density of site was allowed to vary continuously with the radius of the tumor. The density of lattice sites near the center of the lattice was significantly higher than that at the edge. A higher site density corresponds to less real cells per

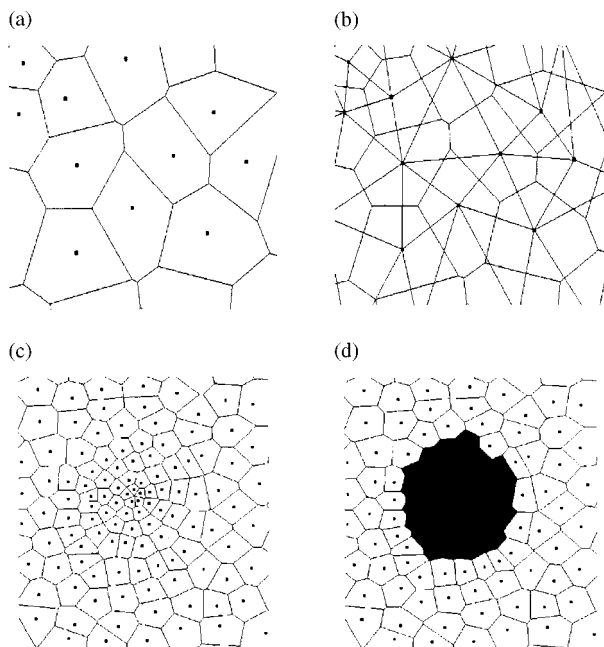


FIG. 3. Two-dimensional space tiled into Voronoi cells. Points represent sites and lines denote boundaries between cells. (a) and (b) depict a very small section of a lattice. (a) shows the Voronoi cells, while (b) shows both the Voronoi cells, along with the Delaunay tessellation. (c) and (d) show a more representative section of the lattice, with the variable density of sites evident. (c) shows the entire lattice section, (d) shows the same section with the darkened cells representing a tumor.

automaton cell, and so to a higher resolution. The higher density at the center enables us to simulate the flat small-time behavior of the Gompertz curve. In the current state of the model, the innermost automaton cells represent roughly 100 real cells, while the outermost automaton cells represent roughly 10^6 real cells. The average distance between lattice sites was described by the following relation:

$$\zeta = \frac{1}{6} r^{2/3}, \quad (2)$$

in which ζ is the average distance between lattice sites and r is the radial position at which the density is being measured. This relation restricts the increase in the number of proliferating cells as the tumor grows. Note the $2/3$ appearing in the exponent, which is intended to reflect a surface-area-to-volume-like relation. This conforms to the diffusion of nutrients through the surface

of the tumor, which is known to be a crucial factor in governing the tumor's growth dynamics (Folkman & Hochberg, 1973).

While an isotropic Voronoi tessellation can be generated from any list of random points, not all point sets are equally reasonable. A purely random distribution of points (the Poisson distribution) will have regions in which the density of points is very high, corresponding to a very small Voronoi cell, and regions with a very low density, corresponding to very large cells. While some variation in the size and shape of cells is important to ensure isotropy, it is biologically unreasonable to have large variations. To solve this problem, a technique common in statistical physics known as the random sequential addition (RSA) process was used (Cooper, 1988). In this technique, as random points are generated, they are tested to ensure that they are not within a given distance of any other point. This eliminates the possibility of high-density clusters, though they can be added later to simulate highly proliferative tumor "hot spots". In addition, it is well known that in the RSA process there is a maximum fraction of space which can be filled. In three-dimensions, this "jamming limit" corresponds to an occupied volume fraction of 0.38. By approaching this density, the possibility of a large low-density area is also eliminated. This technique was adapted for our work to allow the minimum distance between points to vary, giving a list of points suitable for generating a biologically reasonable adaptive lattice. The formula used to do so was

$$R_s = 0.146r^{2/3}, \quad (3)$$

where R_s is the minimum distance between points at distance r from the lattice center.

The list of random points in space was fed to a program written by Ernst Mucke called *detri* (Mucke, 1997). The *detri* program generates the Delaunay triangulation in three spatial dimensions for a given list of points. To test the *detri* program, a second Delaunay program, *del-tree3*, was also downloaded (Devillers, 1996). Both programs were run on the same list of points and the results compared to ensure that they were identical. Because the *detri* program provided a more convenient form of output (listing tetrahedra by

the points' indices rather than the specific coordinates) it was used for the remainder of the work done.

The *detri* program was run on an IBM SP2 parallel computer. Due to memory limitations, the list of sites was divided into sublists. The program was then run on each sublist, generating partial lattices. Culling these partial lattices into a single complete lattice required some care. In order to avoid missing triangles across the divisions between sublists, a significant amount of overlap was included in each sublist. A second challenge, however, are the triangles formed at the edges of each sublist. This led to extra triangles being included in the overall lattice. Because these extra triangles are localized at the subset boundaries, however, it is possible to eliminate them. This is done by generating two different sets of sublists from the same original list and then comparing the two final lattices. Any triangles not found in both lattices are considered to be effects of the division and are discarded. This produces a Delaunay lattice over the entire point set. In order to check the procedure followed here, the division process was done on a point set that could be run in its entirety. The division method gave the same final lattice as when the entire point set was run and so was considered to be accurate.

Once the lattice is generated, the proliferation algorithm can be run. This algorithm is designed to allow a tumor consisting of a few automaton cells, representing roughly 1000 real cells, to grow to a full macroscopic size. An idealized model of a macroscopic tumor is a spherical body consisting of several concentric shells. The inner core, the gray region in Fig. 4, is composed of necrotic cells. The necrotic region has a radius R_n , which is a function of time, t , and is characterized by its distance from the proliferation rim, δ_n . The next shell, the cross-hatched region in the figure, contains cells which are alive but in the G_0 cell-cycle rest state. This is termed the non-proliferative region and is defined in terms of its distance from the edge of the tumor, δ_p . This thickness is the maximum distance from the tumor edge with a high enough nutrient concentration to maintain active cellular division. In real MTS tumors, however, only about one-third of the viable cells increase the tumor size by proliferation [which is

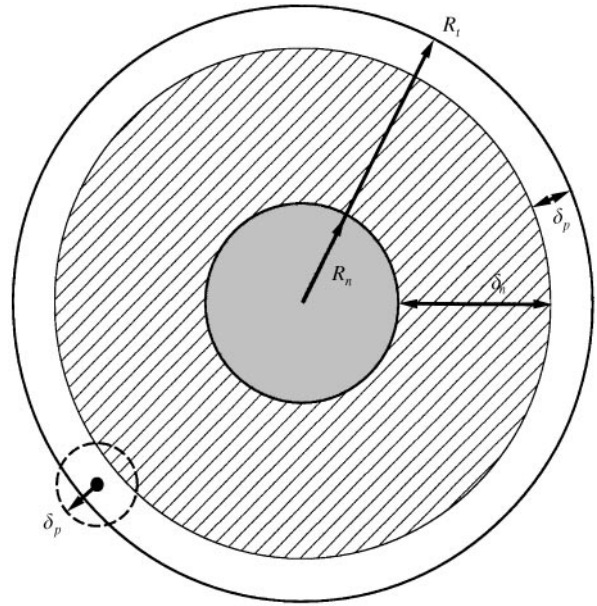


FIG. 4. An idealized tumor. A detailed description of the different regions is contained in the text.

numerically comparable to the growth fraction in macroscopic tumors (Hoshino & Wilson, 1975)]. The others are actively dividing, but the new cells leave the central tumor mass and supposedly trigger invasion into the surrounding tissue (Landry *et al.*, 1981; Freyer & Schor, 1989). Finally, as discussed below, an individual cell can only divide if free space exists within a certain distance of it. This distance must also be δ_p (as defined above) to properly account for the nutrient gradient basis for the transition of cells between the actively dividing and G_0 arrested states. This distance is depicted as a small broken circle in Fig. 4. Both real tumors and our simulated tumors, however, are not perfectly spherical. As such, the values of R_t and R_n vary over the surface of the tumor. The single values used in the algorithm and listed in our results are obtained by averaging the radii of all the cells at the edge of the tumor or of the necrotic region, respectively, according to the relations:

$$R_t = \frac{\sum_{i=1}^{N_p} r_i}{N_p}, \quad (4)$$

$$R_n = \frac{\sum_{i=1}^{N_n} r_i}{N_n}, \quad (5)$$

where N_p denotes the number of cells on the edge of the proliferative region and N_n denotes the number of cells on the edge of the necrotic core.

This definition of proliferative cells allows cells that are not on the immediate edge of the tumor to divide. In order to accommodate these divisions, without allowing discontinuous division, an algorithm which allows for expansive growth via intercellular mechanical stress (IMS) is used. A one-dimensional schematic of IMS growth is depicted in Fig. 5. In part (a) of the figure, cell A is a non-tumorous cell. Non-tumorous cells are treated as empty in the current model, which simply means that, when “filled”, they are considered to have been forced into the surrounding region of indistinguishable non-tumorous cells. Cells B, C, and D are tumor cells which may divide. When cell D attempts to divide, it cannot find an empty space within δ_p and will turn non-proliferative. When cell C attempts to divide it can find cell A and so it will divide. Note that, biologically, cell C actually cannot “see” cell A, but rather senses its location because of the higher nutrient level. Division creates a cell C' which fills the space previously occupied by cell B, which is in turn forced to the space previously filled by cell A. Cell A is regarded as being forced

into the surrounding tissue and disappears (for now) from our consideration. This is the new configuration depicted in part (b) of Fig. 5.

In three spatial dimensions, 1.5 million lattice sites are used. This has been found to be the minimum required to give adequate spatial resolution over the entire range of tumor radii. Naturally, more sites would be desirable, however, practical limits dictate that as few sites as possible be used. The initial tumor is a few automaton cells, representing roughly 1000 real cells, located at the center of the lattice.

In summary, the four key quantities R_t , δ_p , δ_n , and p_d are functions of time calculated within the model. To find them, the simulation utilizes four microscopic parameters: p_0 , a , b and R_{max} . These parameters are linked to the cell-doubling time, the nutritional needs of growth-arrested cells, the nutritional needs of dividing cells, and the effects of confinement pressure, respectively. The quantities are calculated according to the following algorithm.

- Initial setup: The cells within a fixed initial radius of the center of the grid are designated proliferative. All other cells are designated as non-tumorous.
- Time is discretized and incremented, so that at each time step:
 - Each cell is checked for type: non-tumorous or (apoptotic and) necrotic, non-proliferative or proliferative tumorous cells.
 - Non-tumorous cells and tumorous necrotic cells are inert.
 - Non-proliferative cells more than a certain distance, δ_n , from the tumor's edge are turned necrotic. This is designed to model the effects of a nutritional gradient. The edge of the tumor is taken to be the nearest non-tumorous cell.

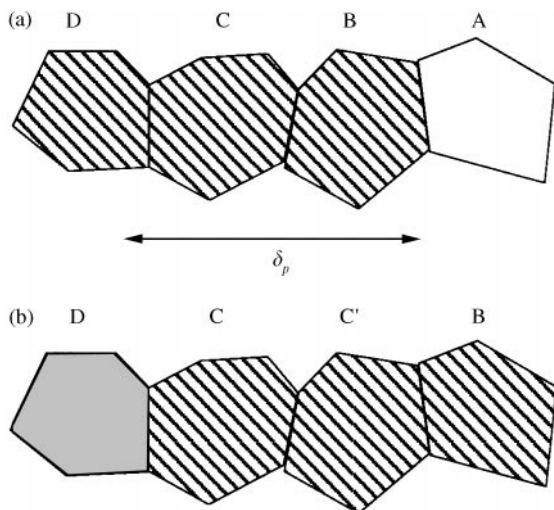


FIG. 5. Schematic of expansive growth via intercellular mechanical stress (IMS). In (a) cell A is non-tumorous, B–D are tumorous and able to divide. (b) Depicts the results of attempted divisions by cells C and D, in which C' is the new cell created by the successful division of C. A full description is contained in the text.

$$\delta_n = aR_t^{2/3}, \quad (6)$$

where a , the base necrotic thickness, is a parameter with units of $(length)^{1/3}$. Note the $2/3$ in the exponent, again indicating a surface-area–volume-type relation.

TABLE 1
*Summary of time-dependent functions and input parameters
 for our model*

Functions within the model (time dependent)	
R_t	Average overall tumor radius
δ_p	Proliferative rim thickness (determines growth fraction)
δ_n	Non-proliferative thickness (determines necrotic fraction)
p_d	Probability of division (varies with time and position)
Parameters (constant inputs to the model)	
p_0	Base probability of division, linked to cell-doubling time
a	Base necrotic thickness, controlled by nutritional needs
b	Base proliferative thickness, controlled by nutritional needs
R_{max}	Maximum tumor extent, controlled by pressure response

—Proliferative cells are checked to see if they will attempt to divide. This is a random process, though the probability of division, p_d , is influenced by the location of the dividing cell (r), reflecting the effects of mechanical confinement pressure. This effect requires the use of an additional parameter, the maximum tumor extent, R_{max} . This probability is determined by the equation:

$$p_d = p_0 \left(1 - \frac{r}{R_{max}} \right). \quad (7)$$

—If a cell attempts to divide, it will search for sufficient space for the new cell beginning with its nearest neighbors and expanding outwards until either an empty (non-tumorous) space is found or nothing is found within the proliferation radius, δ_p . The radius searched is calculated as

$$\delta_p = bR_t^{2/3}, \quad (8)$$

where b , the base proliferative thickness, is a parameter with units of $(length)^{1/3}$.

—If a cell attempts to divide but cannot find space it is turned into a non-proliferative cell.

(The above two steps constitute the re-definition of the proliferative to non-

proliferative transition that is one of the most important new features of the model. They allow a larger number of cells to divide, since cells no longer need to be on the outermost surface of the tumor to divide. In addition, it ensured that cells which cannot divide are correctly labeled as such.)

- After a predetermined amount of time has been stepped through, the volume and radius of the tumor can be plotted as a function of time.
- The type of cell contained in each grid can also be saved at given times.

Table 1 summarizes the important time-dependent functions calculated by the algorithm and the constant parameters used.

4. Results

The simulation has been compared with available experimental data for an untreated GBM tumor from medical literature. The parameters compared were cell number, growth fraction, necrotic fraction and volumetric doubling time. Medically, these data are used to determine a tumor's malignancy and the prognosis for its future growth. Because it is impossible to determine the exact time a tumor began growing, the medical data are listed at fixed radii. The different cell fractions used were extrapolated from the spheroid level and compared to data published for

cell fractions at macroscopic stages. Previous research has shown that the expanding tumor increases both its cell loss (through necrosis/apoptosis and invasion) and its quiescent cell population (G_0/G_1 arrested) due to a declining gradient of nutritional elements towards the center of the rapidly growing avascular mass (Folkman & Hochberg, 1973; Durand, 1976; Landry *et al.*, 1981; Freyer & Sutherland, 1986; Mueller-Klieser *et al.*, 1986; Rotin *et al.*, 1986; Freyer & Schor, 1989). At advanced tumor stages, volumetric growth slows down mostly due to the declining growth fraction (GF), an increasing cell loss and G_0 -fraction (Turner & Weiss, 1980; Bauer *et al.*, 1982; Freyer & Sutherland, 1985) caused by a lack of nutrition as well as an increasing confinement pressure.

Summarized in Table 2 is the comparison between simulation results and data (experimental, as well as clinical) taken from the medical literature. For macroscopic glial tumors (the latter three time points) cell numbers, tumor volumes, and volumetric doubling time measurements, including growth and necrotic fractions and survival times, were taken from Hoshino & Wilson (1975); Hoshino & Wilson (1979), Yamashita & Kuwabara (1983), Yoshii *et al.* (1986), Alvord (1995), Blankenberg *et al.* (1995), Pierallini *et al.* (1996) and Burgess *et al.* (1997). For the microscopic spheroid level, doubling times as well as viable rim diameter, rim cell fractions, necrotic fractions and cell shedding

data were taken from Haji-Karim & Carlsson (1978), Carlsson *et al.* (1983), Carlsson & Acker (1988), Freyer & Schor (1989) and Landry *et al.* (1981). Since it is virtually impossible to measure total cell numbers in macroscopic tumor (the latter three time points), we have used the volume-doubling times to estimate the number of cells in the tumors, including at the microscopic (MTS) level. This method, however, leads to a rather high cell number at the MTS level [experimental values range from 10^4 to 10^5 cells (Freyer, 1988, 1998)]. In a few cases, glioma MTS data were not available and thus data from other well-characterized cell lines were used after careful evaluation. On the whole, the simulation data reproduce the test case very well. The virtual patient would die roughly 11 months after the tumor radius reached 5 mm and 3.5 months after the expected time of diagnosis. The fatal tumor volume is about 65 cm^3 .

These data were created using a tumor which was grown from an initial radius of 0.1 mm. The following parameter set was used:

$$p_0 = 0.192, \quad a = 0.42 \text{ mm}^{1/3}, \quad b = 0.11 \text{ mm}^{1/3},$$

$$R_{max} = 37.5 \text{ mm.}$$

This value of p_0 corresponds to a cell-doubling time of 4.0 days, which is reasonable for high-grade glial tumors (Hoshino & Wilson, 1979;

TABLE 2

Comparison of test case data and simulation results (Sim). Note that the time row is simulation data only and is taken from the start of the simulation not from the theoretical start of the tumor growth

		Spheroid	Detect. lesion	Diagnosis	Death
Time	Sim.	Day 69	Day 223	Day 454	Day 560
Radius	Data	0.5 mm	5 mm	18.5 mm	25 mm
	Sim.	0.5	5	18.5	25
Cell no.	Data	10^6	10^9	5×10^{10}	10^{11}
	Sim.	7×10^5	6×10^8	4×10^{10}	9×10^{10}
Growth fraction	Data	36%	30%	20%	9%
	Sim.	35	30	18	11
Necrotic fraction	Data	46%	49%	55%	60%
	Sim.	38	53	58	63
Volume-doubling time	Data	6 days	45 days	70 days	105 days
	Sim.	9	36	68	100

Pertuiset *et al.*, 1985). The a and b parameters have been chosen to give a growth history that quantitatively fits the test case. As discussed below, the specification of these parameters corresponds to the specification of a clonal strain. This is manifested in qualitative behavior that is independent of the choice of the a and b parameters, but quantitative behavior that is strongly affected by them. The R_{max} parameter was similarly chosen to match the test case history. In this case, however, the fit is relatively insensitive to the value of R_{max} , as long as the parameter is somewhat larger than the fatal radius in the test case. Indeed, the fit is relatively insensitive to the exact form of eqn (7) in general.

Since a three-dimensional CA image is difficult to visualize, cross sections of the tumors are shown instead. The growth of the tumor can be followed graphically over time in Fig. 6. It depicts the central cross section of the tumor, with the convention that necrotic cells are labeled with black, non-proliferative tumorous cells with light gray and proliferative tumor cells with dark gray. Note that the plotted points are not intended to depict the exact shape of the Voronoi cells, but rather just their positions. Figure 7 depicts

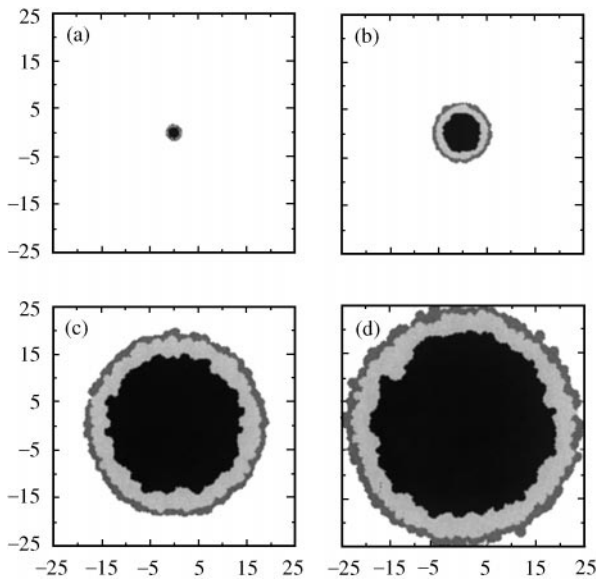


FIG. 6. The development of the cross-central section of a tumor in time. (a) corresponds to the tumor spheroid stage, (b) to the first detectable lesion, (c) to diagnosis and (d) to death. The dark-gray outer region is comprised of proliferating cells, the light-gray region is non-proliferative cells and the black region is necrotic cells. The scales are in millimeters.

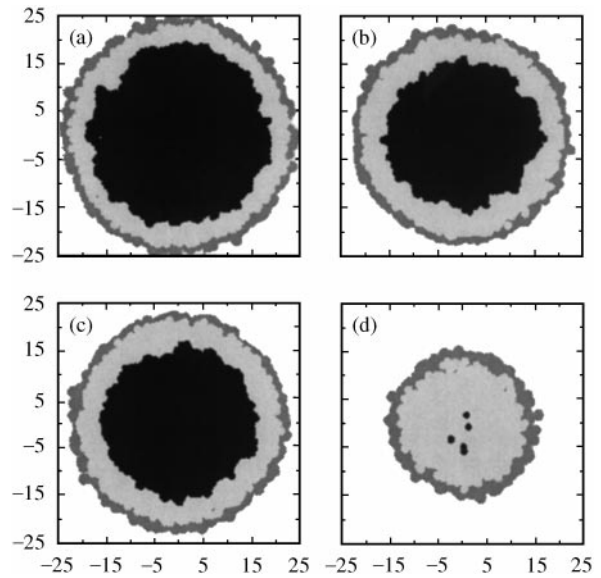


FIG. 7. Cross sections of a fully developed tumor (radius = 25 mm). (a) The central slice. (b) and (c) are taken 10 mm from the center. (d) Taken 20 mm from the center, on the same side as (b). The dark-gray region is proliferating cells, the light-gray region non-proliferative cells and the black region necrotic cells. The scales are in millimeters.

several cross sections taken at different positions from within a single fully developed tumor. As expected in this idealized case, the tumor is essentially spherical, within a small degree of randomness. The high degree of spherical symmetry ensures that the central cross section is a representative view. The volume and radius of the developing tumor are shown vs. time in Fig. 8. Note that the virtual patient dies while the untreated tumor is in the rapid growth phase.

While these results confirm that the algorithm is able to reproduce a very idealized case, they do not illustrate its ability to model more complex situations. As mentioned in the Introduction, one such complexity is the inclusion of multiple distinct tumor clones. An interesting question we have begun to address is that of the emergence of a clonal population from a small mutated hot spot in the original cell population. To address this, a second strain is defined by the parameter set:

$$p_0 = 0.384, \quad a = 0.42 \text{ mm}^{1/3}, \quad b = 0.11 \text{ mm}^{1/3},$$

$$R_{max} = 37.5 \text{ mm}.$$

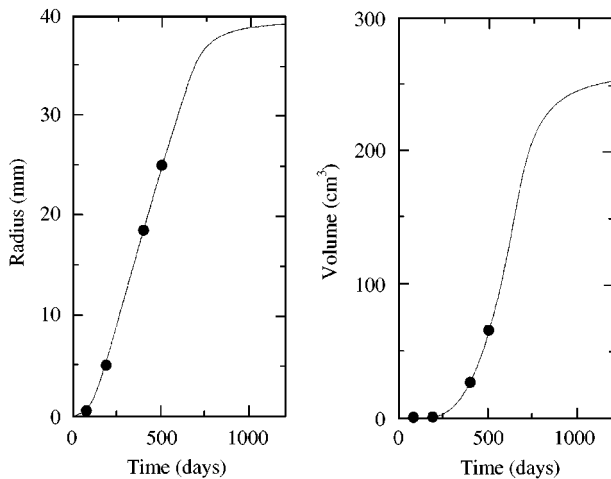


FIG. 8. Plots of the radius and volume of the tumor versus time. The lines correspond to simulation predictions, using the first parameter set given in the text. The plotted points reflect the test case derived from the medical literature. A quantitative comparison of the simulation with the test case is given in Table 2.

The second strain is a more rapidly dividing clone than the first, parental strain defined above. The increase in p_0 gives a decreased cell-doubling time (1.7 vs. 4 days in the primary strain), chosen to reflect the degree of heterogeneity between different clonal strains. This example corresponds to the emergence of a more rapidly dividing malignant parental strain and thereby models the “progression pathway” of GBM tumors from less malignant precursors (Lang *et al.*, 1994). This simulation begins in the same way as the previous one, with a very small tumor, composed entirely of cells of the primary strain. This tumor is then allowed to grow until it reaches a predefined overall radius of 3.8 mm. A mutated hot spot is then introduced as a single, randomly selected, CA cell (corresponding to roughly 10^5 real cells, i.e. the size of a spheroid) changing from the primary strain to the secondary strain. This represents the appearance of the second genotype in roughly 0.01% of the viable tumor cells at that time, assuming monoclonal expansion. At this time we do not distinguish between random mutational activity (intrinsic) or environmentally caused mutational stresses. Figure 9 depicts the development of the secondary strain (shown in blue) in the cross-sectional slice nearest the appearance of the mutation, which is displaced from

the tumor center by roughly 2.5 mm in this case. To aid in distinguishing between strains, cells of the primary clonal strain (dark gray in Fig. 6) have been colored red, while the non-proliferative cells (light gray in previous figures) have been colored yellow. A bulge near the initial position of mutation appears soon after the mutation occurs. This corresponds to a more rapidly advancing tumor rim due to a higher local proliferation rate. This higher proliferation rate also leads to additional cells being shed per unit of time, which in turn leads to a higher invasive potential towards this area. Gradually, the secondary strain overtakes the primary strain and comes to dominate the entire tumor. This example shows the spatial evolution of a secondary tumor population. From such a simulation, it is possible to consider the effects of mutations on the shape and location of a tumor. In this simulation, the secondary strain overtakes the primary strain sufficiently rapidly so that the center of mass of the entire tumor shifts considerably from its original location. In addition, the bulge created by the more rapidly advancing front increases the surface-area-to-volume ratio of the tumor, thereby increasing the growth fraction and causing the tumor growth to accelerate more than would be the case if the tumor remained spherical.

Currently, we are exploring the survival probability of a secondary strain as a function of the number of cells that have mutated and the competitive advantage it enjoys as well as the position within the tumor at which the second strain arises. Given too small an advantage, the second strain will be quickly overwhelmed by the much more common primary strain and will likely disappear. Preliminary results show that for a fairly small mutation, like the one considered here, a large competitive advantage in doubling time is required (of the order of a factor of two), for the secondary population to survive. In biomedical terms, the tumor is “searching” for the best suited heterogeneous pattern, i.e. the genotypes and phenotypes (considering gene expression changes, along with mutations) that are optimal relative to the tumor’s growth rate. The current model focuses on the importance of growth-promoting genetic combinations. From a biological perspective, the model incorporates selection pressures leading to the dominance of the clonal

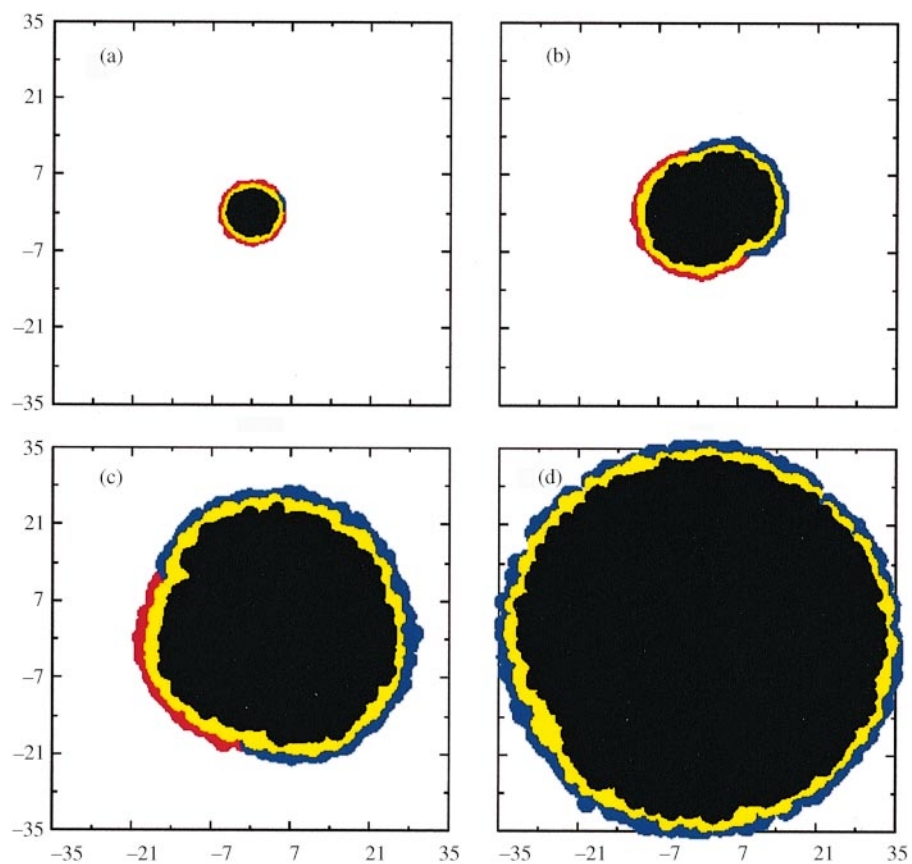


FIG. 9. Cross-section of a tumor, showing the emergence and eventual dominance of a more rapidly growing secondary strain. The red region corresponds to proliferating cells of the primary strain (darker gray in Figs 6 and 7), the blue region to those of the secondary strain, while the yellow (light gray in previous figures) and black regions correspond to non-proliferative and necrotic cells of either strain, respectively. The cross-sections are taken 2.5 mm from the tumor's central plane. (a) Depicts the tumor roughly 1 month after the initial mutated CA cell was introduced in the simulation, (b) 5 months after the mutation, (c) 10 months after the mutation, and (d) 20 months after the mutation. Note that the tumor origin is located at $(0, 0)$, but because of the mutation, the center of mass of the tumor shifts substantially from this location, before being forced back by the boundary conditions.

population best suited to the tumor's environment. Realistically, environmental influences show spatial heterogeneity and as such will not necessarily lead to the dominance scenario depicted here, but rather may lead to a tumor with multiple, coexisting tumor clones (i.e. the hallmark of GBM tumors), each best suited to their local environment.

5. Discussion and Conclusions

Substantial progress has been made in the various specialized areas of cancer research. Yet the complexity of the disease on both the single cell level as well as the multicellular tumor stage has led to the first attempts to describe tumors as complex, dynamic, self-organizing biosystems, rather than merely focusing on single features (Bagley *et al.*, 1989; Schwab & Pienta, 1996; Coffey, 1998; Waliszewski *et al.*, 1998). To begin to understand the complexity of the proposed system, novel simulations must be developed, incorporating concepts from many scientific areas such as cancer research, statistical mechanics, applied mathematics and nonlinear dynamical systems.

To our knowledge, this is the first three-dimensional cellular automaton model of solid tumor growth, which realistically models the macroscopic behavior of a malignant tumor as a function of time using predominantly microscopic parameters. This four-parameter model predicts the composition and dynamics of malignant brain tumor proliferation at selected clinically relevant time points in agreement with experimental and clinical data. From a modeling perspective, this is also the first use of the Voronoi tessellation to study tumor growth in a cellular automaton. The use of a variable density lattice enables the simulation of tumor growth over nearly three orders of magnitude in radius. Finally, the ability of internal cells to divide represents a physiologically more realistic situation and changes the proliferative dynamics from previous models.

In addition, the discrete nature of our model enables us to directly simulate more complex physiological situations with only minor alterations. Examples include regional differences in structural confinement and the influence of envi-

ronmental factors, such as blood vessels. The impact of surgical procedures or other treatments can also be modeled. Further, we can currently include the hallmark of GBM tumors—heterogeneity—by using tumorous subpopulations with different growth behaviors (Giangaspero & Burger, 1983; Burger & Kleihues, 1989; Paulus & Pfeiffer, 1989). These tumor subpopulations represent a clear step forward from previous “monoclonal” (single population) models. Environmental stresses are known to exert a strong influence on tumor growth (Helmlinger *et al.*, 1997). These stresses can both cause genetic variations, and so increase the number of subpopulations, and select for the most fit tumor subpopulation. It is this diversity in structure and function which enables tumors to react locally and globally. It is important to mention that, according to this concept, systemic tumoral growth increases both intrinsic and extrinsic stress and therefore leads to a higher selection pressure and mutational probability. Since this may advance tumor progression, it clearly argues against Foulds' rule III (that tumor growth and progression are independent) (Foulds, 1954; Rubin, 1994). In the next iteration of the model, we will simulate the conditions which create regional genetic instability and study the effect of specific mutations in tumor cells on the macroscopic growth of tumors. Such information could allow tumor biopsies, which are currently regionally limited, to be put into the context of an evolving system. This will lead to important information about intratumoral competition and cooperation and how tumors adapt to maintain their fitness in the environment they are presented (Greenspan, 1976; Axelrod & Hamilton, 1981; Gatenby, 1996).

Another important step on our way to a complex dynamic tumor model is the specific inclusion of the other key feature of tumors, namely single cell invasion. The current model only includes such an effect implicitly. Active cell motility is a crucial feature, not only because of its local disruptive capacity, but also because of its significance to treatment. If a solid tumor is removed, these invasive cells, which would be left behind, can eventually cause recurrence of the tumor. We are currently working to theoretically assess the factors which may drive some of the

structural elements within the invasive network, in accordance with a proposed deterministic chaos principle (Habib *et al.*, unpublished data). The spatial distribution of these factors will also depend on the heterogeneous intercellular space. While this space is not included in the current work, it will be properly accounted for in further work.

In conclusion, such complex interdisciplinary models are likely to lead to insights within cancer research and into complex biosystems in general. Such insights hold promise for increasing our understanding of tumors as *self-organizing systems*, which in turn may have significant impact both on cancer research and on clinical practice. By no means does this model claim such completeness. It is instead a first, but promising, step towards advanced modeling techniques treating tumors as complex dynamic systems.

S.T. gratefully acknowledges the Guggenheim Foundation for his Guggenheim fellowship to conduct this work. This work has also been supported in part by grants CA84509 and CA69246 from the National Institutes of Health. Calculations were carried out on an IBM SP2, which was kindly provided by the IBM Corporation (equipment grant to Princeton University for the Harvard-Princeton Tumor Modeling Project). The technical assistance provided by Drs Kirk E. Jordan and Gyan V. Bhanot of the IBM T.J. Watson Labs is gratefully acknowledged. The authors would also like to thank Drs Stuart A. Kauffman of the Santa Fe Institute for Complex Science, Jerome B. Posner of Memorial Sloan Kettering Cancer Center, Michael E. Berens of the Barrows Neurological Institute and H.J. Reulen of the University of Munich Neurosurgical Department for valuable discussions.

REFERENCES

- ADAM, J. A. (1986). A simplified mathematical model of tumour growth. *Math. Biosci.* **81**, 229–242.
- ALVORD, E. C. (1995). Patterns of growth of gliomas. *Am. J. Neuroradiol.* **16**, 1013–1017.
- ANNEGERS, J. F., SCHOENBERG, B. D., OKAZAKI, H. & KURLAND, L. T. (1981). Epidemiologic study of primary intracranial neoplasms. *Arch. Neurol.* **38**, 217–219.
- AXELROD, R. & HAMILTON, W. D. (1981). The evolution of cooperation. *Science* **211**, 1390–1396.
- BAGLEY, R. J., FARMER, J. D., KAUFFMAN, S. A., PACKARD, N. H., PERELSON, A. S. & STADNYK, I. M. (1989). Modeling adaptive biological systems. *Biosystems* **23**, 113–138.
- BAUER, K. D., KENG, P. C. & SUTHERLAND, R. M. (1982). Isolation of quiescent cells from multicellular tumor spheroids using centrifugal elutriation. *Cancer Res.* **42**, 72–78.
- BLACK, P. M. (1991). Brain tumors, Part 2. *N. Engl. J. Med.* **324**, 1555–1564.
- BLANKENBERG, F. G., TEGLITZ, R. L., ELLIS, W., SALAMAT, M. S., MIN, B. H., HALL, L., BOOTHROYD, D. B., JOHNSTONE, I. M. & ENZMANN, D. R. (1995). The influence of volumetric doubling time, DNA ploidy, and histological grade on the survival of patients with intracranial astrocytomas. *Am. J. Neuroradiol.* **16**, 1001–1012.
- BRUNTON, G. F. & WHELDON, T. E. (1977). Prediction of the complete growth pattern of human multiple myeloma from restricted initial measurements. *Cell Tissue Kinet.* **10**, 591–594.
- BURGER, P. C. & KLEIHUES, P. (1989). Cytologic composition of the untreated glioblastoma with implications for evaluation of needle biopsies. *Cancer* **63**, 2014–2023.
- BURGER, P. C., HEINZ, E. R., SHIBATA, T. & KLEIHUES, P. (1988). Topographic anatomy and CT correlations in the untreated glioblastoma multiforme. *J. Neurosurg.* **68**, 698–704.
- BURGER, P. C., SCHOLD, P. J., SMITH Jr., K. R., ODOM, G. L., CRAFTS, D. C. & GIANGASPERO, F. (1983). Computerized tomographic and pathologic studies of the untreated, quiescent, and recurrent glioblastoma multiforme. *J. Neurosurg.* **58**, 159–169.
- BURGESS, P. K., KULESA, P. M., MURRAY, J. D. & ALVORD, E. C. (1997). The interaction of growth rates and diffusion coefficients in a three-dimensional mathematical model of gliomas. *J. Neuropathol. Exp. Neurol.* **56**, 704–713.
- BYRNE, H. M. & CHAPLAIN, M. A. J. (1998). Necrosis and apoptosis: distinct cell loss mechanisms in a mathematical model of avascular tumour growth. *J. Theor. Med.* **1**, 223–235.
- CARLSSON, J. & ACKER, H. (1988). Relations between pH, oxygen partial pressure and growth in cultured cell spheroids. *Int. J. Cancer* **42**, 715–720.
- CARLSSON, J., NILSSON, K., WESTERMARK, B., PONTEN, J., SUNDBLAD, C., LARSSON, E., BERGH, J., PAHLMAN, S., BUSCH, C. & COLLINS, V. P. (1983). Formation and growth of multicellular spheroids of human origin. *Int. J. Cancer* **31**, 523–533.
- CHAPLAIN, M. A. J. & SLEEMAN, B. D. (1993). Modelling the growth of solid tumours and incorporating a method for their classification using nonlinear elasticity theory. *J. Math. Biol.* **31**, 431–473.
- COFFEY, D. S. (1998). Self-organization, complexity and chaos: the new biology for medicine. *Nat. Med.* **4**, 882–885.
- COOPER, D. W. (1988). Random sequential packing simulations in 3 dimensions for spheres. *Phys. Rev. A* **38**, 522–524.
- CRUYWAGEN, G. C., WOODWARD, D. E., TRACQUI, P., BARTOO, G. T., MURRAY, J. D. & ALVORD, E. C. (1995). The modelling of diffusive tumours. *J. Biol. Sys.* **3**, 937–945.
- DEVILLERS, O. (1996). <http://www.inria.fr/prisme/logiciel/del-tree.html>
- DÜCHTING, W. & VOGELSAENGER, T. (1985). Recent progress in modelling and simulation of three-dimensional tumor growth and treatment. *Biosystems* **18**, 79–91.
- DURAND, R. E. (1976). Cell cycle kinetics in an in vitro tumor model. *Cell Tissue Kinet.* **9**, 403–412.
- EARNEST IV, F., KELLY, P. J., SCHEITHAUER, B. W., KALL, B. A., CASCINO, T. L., EHMAN, R. L., FORBES, G. S. & AXLEY, P. L. (1988). Cerebral astrocytomas: histopathological correlation of MR and CT contrast enhancement with stereotactic biopsy. *Radiology* **166**, 823–827.

- FOLKMAN, J. & HOCHBERG, M. (1973). Self-regulation of growth in three dimensions, *J. Exp. Med.* **138**, 745–753.
- FOULDS, L. (1954). The experimental study of tumor progression: a review. *Cancer Res.* **14**, 327–339.
- FREYER, J. P. (1988). Role of necrosis in regulating the growth saturation of multicellular spheroids. *Cancer Res.* **48**, 2432–2439.
- FREYER, J. P. (1998). Decreased mitochondrial function in quiescent cells isolated from multicellular tumor spheroids. *J. Cell. Physiol.* **176**, 138–149.
- FREYER, J. P. & SCHOR, P. L. (1989). Regrowth kinetics of cells from different regions of multicellular spheroids of four cell lines. *J. Cell. Physiol.* **138**, 384–392.
- FREYER, J. P. & SUTHERLAND, R. M. (1985). A reduction in the in situ rates of oxygen and glucose consumption of cells in the EMT6/Ro spheroids during growth. *J. Cell. Physiol.* **124**, 516–524.
- FREYER, J. P. & SUTHERLAND, R. M. (1986). Regulation of growth saturation and development of necrosis in EMT6/Ro multicellular spheroids by the glucose and oxygen supply. *Cancer Res.* **46**, 3504–3512.
- GATENBY, R. A. (1996). Applications of competition theory to tumour growth: implications for tumour biology and treatment. *Eur. J. Cancer* **32A**, 722–726.
- GIANGASPERO, F. & BURGER, P. C. (1983). Correlations between cytologic composition and biologic behavior in the glioblastoma multiforme: a postmortem study of 50 cases. *Cancer* **52**, 2320–2333.
- GIESE, A., LOO, M. A., TRAN, N., HASKETT, D., COONS, S. W. & BERENS, M. E. (1996). Dichotomy of astrocytoma migration and proliferation. *Int. J. Cancer* **67**, 275–282.
- GREENSPAN, H. P. (1976). On the growth and stability of cell cultures and solid tumors. *J. theor. Biol.* **56**, 229–242.
- HAIJ-KARIM, M. & CARLSSON, J. (1978). Proliferation and viability in cellular spheroids of human origin. *Cancer Res.* **38**, 1457–1464.
- HAROSKE, G., DIMMER, V., STEINDORF, D., SCHILLING, U., THEISSIG, F. & KUNZE, K. D. (1996). Cellular sociology of proliferating tumor cells in invasive ductal breast cancer. *Analyt. Quant. Cytol. Histol.* **18**, 191–198.
- HEMLINGER, G., NETTI, P. A., LICHTENBELD, H. C., MELDER, R. J. & JAIN, R. K. (1997). Solid stress inhibits the growth of multicellular tumor spheroids. *Nat. Biotechnol.* **15**, 778–783.
- HOSHINO, T. & WILSON, C. B. (1975). Review of basic concepts of cell kinetics as applied to brain tumors. *J. Neurosurg.* **42**, 123–131.
- HOSHINO, T. & WILSON, C. B. (1979). Cell kinetic analyses of human malignant brain tumors (gliomas). *Cancer* **44**, 956–962.
- KAUFFMAN, S. A. (1984). Emergent properties in random complex automata. *Physica* **10D**, 145–156.
- KELLY, P. J., DUMAS-DAVENPORT, C., KISPERT, D. B., KALL, B. A., SCHEITHAUER, B. W. & ILLIG, J. J. (1987). Imaging-based stereotactic serial biopsies in untreated intracranial glial neoplasms. *J. Neurosurg.* **66**, 865–874.
- KISS, R., CAMBY, I., SALMON, I., VAN HAM, P., BROTCHE, J. & PASTEELS, J. (1995). Relationship between DNA ploidy level and tumor sociology behavior in 12 nervous cell lines. *Cytometry* **20**, 118–126.
- KRAUS, M. & WOLF, B. (1993). Emergence of self-organization in tumor cells: relevance for diagnosis and therapy. *Tumor Biol.* **14**, 338–353.
- LANDRY, J., FREYER, J. P. & SUTHERLAND, R. M. (1981). Shedding of mitotic cells from the surface of multicell spheroids during growth. *J. Cell. Physiol.* **106**, 23–32.
- LANG, F. F., MILLER, D. C., KOSLOV, M. & NEWCOMB, E. W. (1994). Pathways leading to glioblastoma-multiforme: a molecular analysis of genetic alteration in 65. *J. Neurosurg.* **81**, 427–436.
- MARUSIC, M., BAJZER, Z., FREYER, J. P. & VUC-PAVLOVIC, S. (1994). Analysis of growth of multicellular tumour spheroids by mathematical models. *Cell Prolif.* **27**, 73–94.
- MUCKE, E. (1997). <http://www.geom.umn.edu/locate/cglist/GeomDir>.
- MUELLER-KLIESER, W. (1997). Three-dimensional cell cultures: from molecular mechanisms to clinical applications. *Am. J. Physiol.* **273**, C1109–C1123.
- MUELLER-KLIESER, W., FREYER, J. P. & SUTHERLAND, R. M. (1986). Influence of glucose and oxygen supply conditions on the oxygenation of multicellular spheroids. *Br. J. Cancer* **53**, 345–353.
- NAZZARO, J. M. & NEUWELT, E. A. (1990). The role of surgery in the management of supratentorial intermediate and high-grade astrocytomas in adults. *J. Neurosurg.* **73**, 331–344.
- NORTON, L. (1988). A Gompertzian model of human breast cancer growth. *Cancer Res.* **48**, 7067–7071.
- OKABE, A., BOOTS, B. & SUGIHARA, K. (1992). *Spatial Tessellations*. New York: Wiley.
- PAULUS, W. & PFEIFFER, J. (1989). Intratumoral histologic heterogeneity of gliomas: a quantitative study. *Cancer* **64**, 442–447.
- PERTUISSET, B., DOUGHERTY, D., CROMEYER, C., HOSHINO, T., BERGER, M. & ROSENBLUM, M. L. (1985). Stem cell studies of human malignant brain tumors. Part 2.: Proliferation kinetics of brain-tumor cells in vitro in early-passage cultures. *J. Neurosurg.* **63**, 426–432.
- PERUMPANANI, A., SHERRATT, J. A., NORBURY, J. & BYRNE, H. M. (1996). Biological inferences from a mathematical model for malignant invasion. *Invasion Metastasis* **16**, 209–221.
- PIERALLINI, A., BONAMIMI, M., OSTI, M. F., PANTANO, P., PALMEGGIANI, F., SANTORO, A., ENRICI, R. M. & BOZZAO, L. (1996). Supratentorial glioblastoma: neuroradiological findings and survival after surgery and radiotherapy. *Neuroradiology* **38**, S26–S30.
- PRESTON JR., K. & SIDERITS, R. (1992). New techniques for three-dimensional data analysis in histopathology. *Analyt. Quant. Cytol. Histol.* **14**, 398–406.
- QI, A. S., ZHENG, X., DU, C. Y. & AN, B. S. (1993). A cellular automaton model of cancerous growth. *J. theor. Biol.* **161**, 1–12.
- ROTH, D., ROBINSON, B. & TANNOCK, I. F. (1986). Influence of hypoxia and an acidic environment on the metabolism and viability of cultured cells: potential implications for cell death in tumors. *Cancer Res.* **46**, 2821–2826.
- RUBIN, H. (1994). Experimental control of neoplastic progression in cell populations: Foulds' rules revisited. *Proc. Nat. Acad. Sci. U.S.A.* **91**, 6619–6623.
- SCHIFFER, D., CAVALLA, P., DUTTO, A. & BORSOTTI, L. (1997). Cell proliferation and invasion in malignant gliomas. *Anticancer Res.* **17**, 61–70.

- SCHWAB, E. D. & PIANTA, K. J. (1996). Cancer as a complex adaptive system. *Med. Hypotheses* **47**, 235–241.
- SELKER, R. G., MENDELOW, H., WALKER, M., SHEPTAK, P. E. & PHILIPS, J. G. (1982). Pathological correlation of CT ring in recurrent, previously treated gliomas. *Surg. Neurol.* **17**, 251–254.
- SHERRATT, J. A. & NOWAK, M. A. (1992). Oncogenes, anti-oncogenes and the immune response to cancer: a mathematical model. *Proc. Roy. Soc. London [B]* **248**, 261–271.
- SILBERGELD, D. L. & CHICOINE, M. R. (1997). Isolation and characterization of human malignant glioma cells from histologically normal brain. *J. Neurosurg.* **86**, 525–531.
- SMOLLE, J. (1998). Cellular automaton simulation of tumour growth—equivocal relationships between simulation parameters and morphologic pattern features. *Analyt. Cell. Pathol.* **17**, 71–82.
- SMOLLE, J. & STETTNER, H. (1993). Computer simulation of tumour cell invasion by a stochastic growth model. *J. theor. Biol.* **160**, 63–72.
- STEEL, G. G. (1977). *Growth Kinetics of Tumors*. Oxford: Clarendon Press.
- SUH, O. & WEISS, L. (1984). The development of a technique for the morphometric analysis of invasion in cancer. *J. theor. Biol.* **107**, 547–561.
- SUTHERLAND, R. M. (1988). Cell and environment interactions in tumor microregions: the multicell spheroid model. *Science* **240**, 177–184.
- TRACQUI, P. (1995). From passive diffusion to active cellular migration in mathematical models of tumor invasion. *Acta Biotheor.* **43**, 443–464.
- TRACQUI, P., CRUYWAGEN, G. C., WOODWARD, D. E., BARTOO, G. T., MURRAY, J. D. & ALVORD, E. C. (1995). A mathematical model of glioma growth: the effect of chemotherapy on spatio-temporal growth. *Cell Prolif.* **28**, 17–31.
- TURNER, G. A. & WEISS, L. (1980). Some effects of products from necrotic regions of tumours on the in vitro migration of cancer and peritoneal exudate cells. *Int. J. Cancer* **26**, 247–254.
- VAIDYA, V. G. & ALEXANDRO JR., F. J. (1982). Evaluation of some mathematical models for tumor growth. *Int. J. Biomed. Comput.* **13**, 19–35.
- WALISZEWSKI, P., MOLSKI, M. & KONARSKI, J. (1998). On the holistic approach in cellular and cancer biology: nonlinearity, complexity and quasi-determinism of the dynamic cellular network. *J. Surg. Oncol.* **68**, 70–78.
- WARD, J. P. & KING, J. R. (1997). Mathematical modelling of avascular-tumour growth. *IMA J. Math. Appl. Med. Biol.* **14**, 39–69.
- WASSERMAN, R., ACHARYA, R., SIBATA, C. & SHIN, K. H. (1996). A patient-specific in vivo tumor model. *Math. Biosci.* **136**, 111–140.
- WERNER, M. H., PHUPHANICH, S. & LYMAN, G. H. (1995). The increasing incidence of malignant gliomas and primary central nervous system lymphoma in the elderly. *Cancer* **76**, 1634–1642.
- WHITTLE, I. R. (1996). Management of primary malignant brain tumours. *J. Neurol. Neurosurg. Psychiatry* **60**, 2–5.
- WOLFRAM, S. (1984). Cellular automata as models of complexity. *Nature* **311**, 419–424.
- WOODWARD, D. E., COOK, J., TRACQUI, P., CRUYWAGEN, G. C., MURRAY, J. D. & ALVORD, E. C. (1996). A mathematical model of glioma growth: the effect of extent of surgical resection. *Cell Prolif.* **29**, 269–328.
- YAMASHITA, T. & KUWABARA, T. (1983). Estimation of rate of growth of malignant brain tumors by computed tomography scanning. *Surg. Neurol.* **20**, 464–470.
- YOSHII, Y., MAKI, Y., TSUBOI, K., TOMONO, Y., NAKAGAWA, K. & HOSHINO, T. (1986). Estimation of growth fraction with bromodeoxyuridine in human central nervous system tumors. *J. Neurosurg.* **65**, 659–663.